MINERALOGY AND GENESIS OF CLAYS IN POSTMAGMATIC ALTERATION ZONES, MAKURAZAKI VOLCANIC AREA, KAGOSHIMA PREFECTURE, JAPAN

MOTOHARU KAWANO[1] AND KATSUTOSHI TOMITA[2]

[1] Department of Environmental Sciences and Technology, Faculty of Agriculture
Kagoshima University, 1-21-24 Korimoto, Kagoshima 890, Japan

[2] Institute of Earth Sciences, Faculty of Science, Kagoshima University
1-21-35, Korimoto, Kagoshima 890, Japan

Abstract—Two distinct zonal sequences of clay minerals (H- and L-type) were found around silicified rocks in the Makurazaki volcanic area, Kagoshima Prefecture, Japan. The clay mineral sequences from the inner to the outer parts of the alteration aureoles are: 1. H-type, pyrophyllite → dickite → $2M_2$ mica → sudoite → tosudite; and 2. L-type, kaolinite → rectorite → smectite. The structural formula for the sudoite is: $(Al_{1.04}Mg_{1.28}Fe^{3+}_{0.20}Ti_{0.03}Li_{0.01}K_{0.02}Na_{0.01})(OH)_6Al_{2.00}(Si_{3.54}Al_{0.46})O_{10}(OH)_2$. It is characterized by relatively large amounts of Mg and very small amounts of Li. The polytype is identified as IIb. The chemical analysis of tosudite shows that the sample is composed of an interstratification of sudoite-like and beidellite-like layers. The structural formula for rectorite is: $(K_{0.45}Na_{0.19}Ca_{0.01}Mg_{0.01})(Al_{1.81}Fe^{3+}_{0.04}Mg_{0.13}Ti_{0.03})(Si_{3.41}Al_{0.59})O_{10}(OH)_2$, suggesting that the nonexpandable and expandable layers have K-mica-like and beidellite-like compositions, respectively. These clay minerals in the H- and L-type alteration aureoles were formed under relatively high- and low-temperature conditions, respectively, with pH value and K- and Mg-activities increasing as the fluids ascended through the wall rocks.

Key Words—Makurazaki volcanic area, Alteration aureoles, Mode of occurrence, Mineralogical properties, Sudoite, Tosudite, Rectorite.

INTRODUCTION

Gold-bearing silicified ore deposits, the so-called Nansatsu-type gold deposits, are widely distributed in the Makurazaki volcanic area, Kagoshima Prefecture, Japan. These deposits were formed by hydrothermal alteration related to volcanic activity during Miocene–Pliocene time. Many kinds of aluminous clay minerals occur as major alteration products in the hydrothermal alteration aureoles around the silicified rocks. The first description of clay minerals occurring in this area was carried out by Tokunaga (1954) in his study of hydrothermal alteration at the Kasuga mine. He reported that alunite, dickite, and kaolinite occurred in the hydrothermal alteration aureole of the mine. Urashima *et al.* (1981, 1987) described the geology of the Makurazaki area and the gold mineralization of the Nansatsu-type gold deposits. Tomita and Dozono (1973) reported the occurrence of a rectorite-like mineral in this area. Kawano *et al.* (1986) investigated clay mineral sequences in the hydrothermal alteration aureoles of some silicified ore deposits, and reported the following clay minerals sequences from the inner parts to the outer parts of the aureoles: silicified rock → kaolinite → mica/smectite mixed-layer → dioctahedral smectite → trioctahedral clay minerals. The present study reports the results of a detailed investigation of mode of occurrence, mineralogical properties, and probable formation processes of the clay minerals.

GEOLOGICAL SETTING

Figure 1 shows a geological map of the Makurazaki area and the location of the alteration aureoles examined in this study. The Shimanto Group of Cretaceous age are the basement rocks of the area and are exposed in the western parts of this area. The group is composed of sandstone and alterations of shale and sandstone. The strata generally strike N–S and dip 70°E–40°W.

The Nansatsu Group of Miocene–Pliocene age covers the Shimanto group unconformably, and is widely distributed in this area. This group is composed of the Kurigano conglomerate, the Banyasan andesite, and the Pre-Kunimidake andesite, in ascending order. The Kurigano conglomerate consists of cobbles of sandstone, shale, and granite porphyry, and is exposed in the southwestern parts of the area. The Banyasan andesite formation, which consists mainly of hornblende andesitic tuff-breccia and two-pyroxene andesite, is exposed in the western part of the area. The Pre-Kunimidake andesite consists of hornblende andesite, two-pyroxene andesite, and two-pyroxene andesitic tuff-breccia, is distributed mainly around Mt. Kunimidake.

The Middle-Nansatsu volcanic rocks of Pliocene age cover the Nansatsu Group unconformably, and are exposed in the central parts of the area. The volcanic rocks are composed of hornblende andesite lava and hornblende andesitic tuff-breccia.
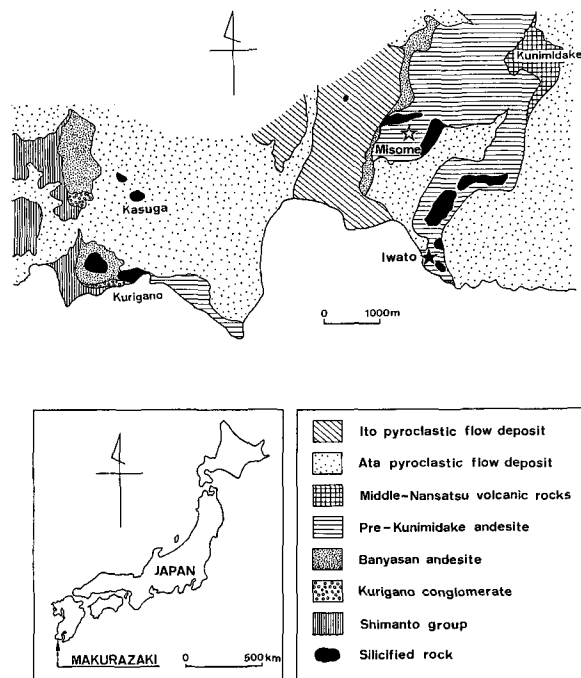
Figure 1. Geological map of the Makurazaki area.

The Ata and Ito pyroclastic flow deposits of Quaternary age are widely distributed in this area.

The hydrothermal, silicified ore deposits were formed in the Nansatsu Group. K-Ar ages for alunites associated with the silicified ore deposits of the Iwato and Kasuga mines are 4.7 and 5.5 m.y., respectively (Izawa *et al.*, 1984). This suggests that the hydrothermal alteration of the Makurazaki area occurred during Pliocene time.

EXPERIMENTAL

The <2-μm fractions of the clay samples obtained by dispersion and sedimentation in distilled water were subjected to chemical analysis, X-ray powder diffraction (XRD), infrared absorption (IR) spectroscopy, thermal analyses and transmission electron microscopy.

Wet chemical analysis utilized the gravimetric method for SiO_2, $H_2O(+)$, and $H_2O(-)$, colorimetric procedures for TiO_2, and atomic absorption spectrometry for the other elements. Exchangeable cations were extracted with 0.1 N $SrCl_2$ solution, and the cation exchange capacity (CEC) measured by determining the amounts of Ca extracted from Ca-saturated material with 0.1 N $SrCl_2$ solution. The XRD analysis was made with a Rigaku diffractometer (30 kV, 100 mA, CuKα radiation) equipped with a graphite monochrometer and 0.5° divergence and scattering slits. The IR spectra were obtained with a Nihonbunko infrared spectrophotometer using KBr pellets. About 1 mg of sample was mixed with 300 mg of KBr powder, and pressed
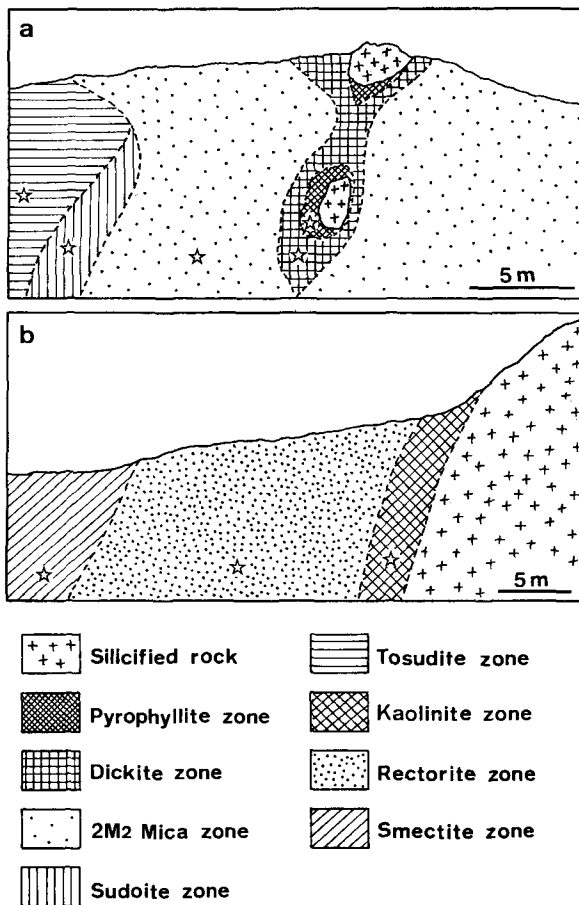

Figure 2. Schematic diagrams of (a) H-type zonal sequence at Misome, and (b) L-type zonal sequence at Iwato. Open stars indicate the samples locations.

into a transparent disc in a vacuum chamber. Thermal analysis was carried out with a Rigaku differential thermal-thermogravimetric analysis (DTA-TGA) apparatus using about 25 mg of air-dried sample. Measurements were made in the range from room temperature to 1100°C, with a heating rate of 10°C/min. The transmission electron micrographs (TEM) were obtained with a Hitachi instrument operated at an accelerating voltage of 200 kV.

MODE OF OCCURRENCE

The clays examined in this study were collected from hydrothermal alteration aureoles in the andesitic rocks at Misome and at Iwato (Figure 1). The mode of occurrence of the clay minerals can be divided into two zonal sequences from the inner to the outer parts of the alteration aureoles: 1. H-type, silicified rock → pyrophyllite → dickite → $2M_2$ mica → sudoite → tosudite; and 2. L-type, silicified rock → kaolinite → rectorite → smectite.

The H-type alteration aureole is observed at Misome

Table 1. Chemical analyses of pyrophyllite.

	1	2	3
SiO_2	64.06	63.57	65.96
Al_2O_3	29.18	29.25	28.25
TiO_2	0.87	0.04	trace
Fe_2O_3	0.63	0.10	0.18
FeO	—	0.12	—
MgO	0.02	0.37	—
CaO	0.00	0.38	—
Na_2O	0.16	trace	—
K_2O	0.07	0.02	—
H_2O (+)	5.28	5.66	5.27
H_2O (−)	0.07	0.66	0.14
Total (%)	100.34	100.17	99.80

(1) Specimen from Makurazaki, Kagoshima Prefecture, Japan. (2) Honami specimen from Nagano Prefecture, Japan (Kodama, 1958). (3) Mariposa County specimen from California, U.S.A. (Deer et al., 1962).

(Figure 2). Pyrophyllite occurs intensively in the innermost parts of the aureole surrounding massive silicified rock. Dickite occurs in the outer parts of the pyrophyllite zone and forms an argillization zone 1–2 m in width. $2M_2$ mica is found most extensively in the outer parts of the dickite zone, 10–20 m in width, and coexisting with large amounts of quartz and pyrite. Sudoite appears in the outer parts of the $2M_2$ mica zone, together with quartz and pyrite. The original rock textures are completely destroyed in the pyrophyllite, dickite, and $2M_2$ mica zones, but remain in the sudoite zone. Tosudite occurs in the outermost parts of the aureole, often coexisting with small amounts of mica, rectorite, and/or smectite.

The L-type alteration aureole is found in andesitic rocks at Iwato (Figure 2). Kaolinite occurs in the innermost parts of the aureole, together with large amounts of quartz and smaller amounts of rectorite. Rectorite is formed in the outer parts of the kaolinite zone, together with quartz and minor amounts of pyrite, kaolinite, and smectite. Smectite appears in the outermost parts of the aureole, coexisting with quartz. Tosudite, in small amounts, is rarely observed.

MINERALOGY OF CLAYS IN THE H-TYPE ALTERATION AUREOLE

Pyrophyllite

Figure 3a shows an XRD pattern of a random mount pyrophyllite sample. Following Brindley and Wardle (1970), the mineral is monoclinic with a d(060) value of 1.492 Å. The chemical analyses of the material, and other pyrophyllite samples from Honami (Kodama, 1958) and Mariposa County (Deer et al., 1962) are given in Table 1. The structural formula is:

$$(Na_{0.02}K_{0.01})(Al_{1.95}Fe^{3+}_{0.03}Ti_{0.04})(Si_{3.87}Al_{0.13})O_{10}(OH)_2.$$
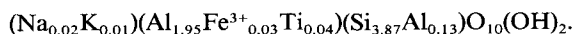
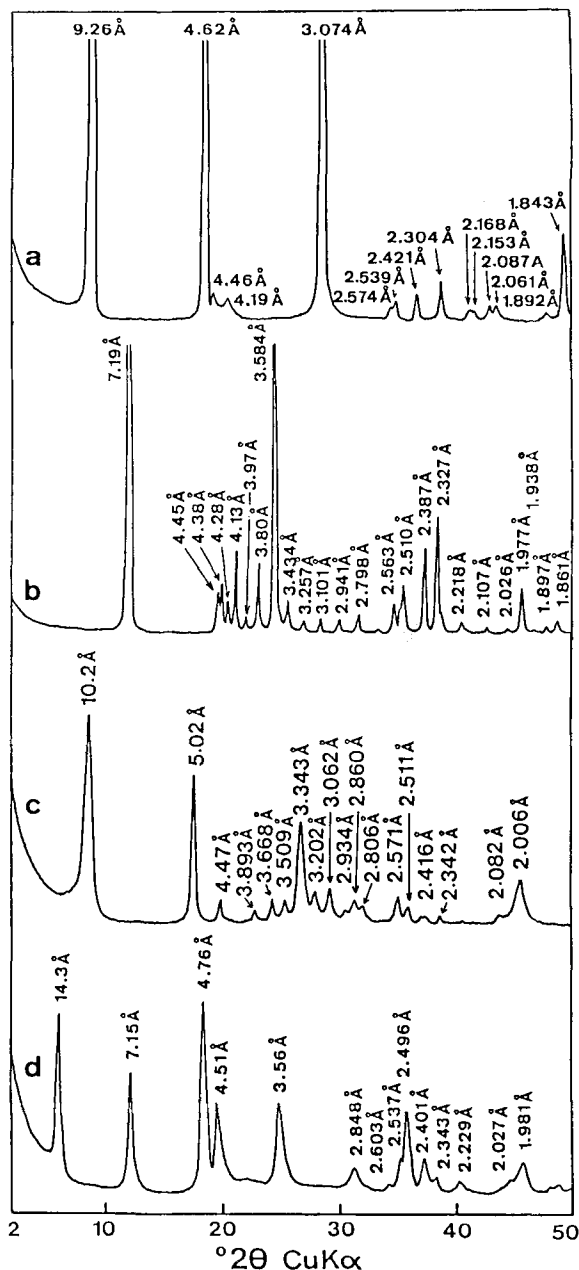The poorly resolved doublets at 2.539–2.574 Å and

Figure 3. X-ray powder diffraction patterns of randomly-oriented (a) pyrophyllite, (b) dickite, (c) $2M_2$ mica, and (c) sudoite.

2.061–2.087 Å, and the presence of octahedral Na, K, Fe^{3+}, and tetrahedral Al, indicate weak isomorphism and structural disorder. The DTA and TGA curves of the sample reveal that the sample dehydroxylated in two steps at 619 and 815°C, and the total weight loss was ~4.8%. The IR spectrum showed a pronounced OH-vibration band at 3680 cm⁻¹ and three Si-O vibrations at 1124, 1071, and 1048 cm⁻¹. The particles exhibit a euhedral lath-shaped habit (Figure 4a).
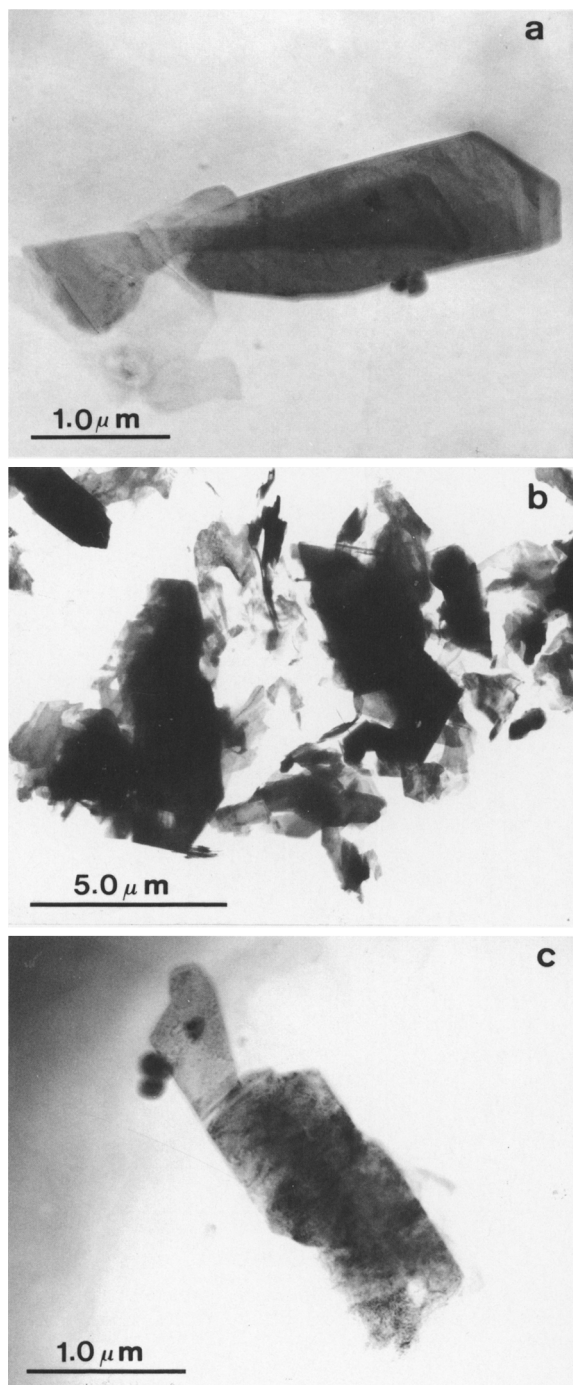
Figure 4. Transmission electron micrographs of (a) pyrophyllite, (b) dickite, and (c) $2M_2$ mica.

Table 2. Chemical analyses of dickite.

	1	2	3
SiO_2	45.75	45.31	46.43
Al_2O_3	38.57	40.17	39.54
TiO_2	0.71	0.00	—
Fe_2O_3	0.52	0.14	0.15
MgO	0.00	trace	0.17
CaO	0.00	0.06	—
Na_2O	0.04	0.24	0.03
K_2O	0.04	0.01	0.02
Li_2O	0.03	—	—
H_2O (+)	14.51	13.89	14.20
H_2O (−)	0.13	0.35	—
Total (%)	100.30	100.11	100.54

(1) Specimen from Makurazaki, Kagoshima Prefecture, Japan. (2) Dickite from Ebara, Hyogo Prefecture, Japan (Ueno, 1964). (3) Dickite from Barkly East, Cape Province, South Africa (Schmidt and Heckroodt, 1959).

refinement are: $a_0 = 5.149(1)$, $b_0 = 8.933(2)$, $c_0 = 14.729(5)$ Å, and $\beta = 103.55(3)°$. The Hinckley index is 1.15, indicating a well-ordered structure. The chemical analysis (Table 2) reveals that the sample contains small amounts of Li ions. The structural formula is:

$$Na_{0.01}K_{0.01}(Al_{3.91}Fe^{3+}_{0.03}Ti_{0.05}Li_{0.01})\text{-}$$
$$(Si_{3.97}Al_{0.03})O_{10}(OH)_8.$$
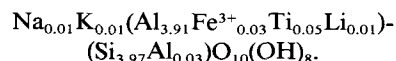
The small amounts of Na, K, Fe^{3+}, Ti, Li, and tetrahedral Al ions indicate weak isomorphism and structural disorder. The IR spectrum exhibits three OH-vibration bands at 3711, 3658, and 3628 cm^{-1}. The absorptions at 3711 and 3658 cm^{-1} originate from hydroxyls located at the surface of the octahedral sheet (Ledoux and White, 1964b; Wada, 1967), and the absorption at 3628 cm^{-1} is due to hydroxyls located between the octahedral and the tetrahedral sheets (Ledoux and White, 1964a, 1964b). The intensities of the absorptions at 3711 (A_{outer}) and 3628 cm^{-1} (A_{inner}) are: $A_{outer} < A_{inner}$, characteristic of dickite (Farmer and Russell, 1964).

Smithson and Brown (1957) studied the dehydroxylation of a well-ordered, pure dickite from Anglesey, Wales, and concluded that the double endotherms they found must be due to the dickite. Schmidt and Heckroodt (1959) studied the dehydroxylation of various size fractions of a dickite from Barkly East. They observed that the 6.3–20 μm size fractions showed double endothermic peaks, the higher temperature peak of which was missing for the <2-μm fractions. They concluded that the double endotherms must be attributed to a particle size effect, and not to the presence of contaminants. In our material, the DTA curve for the <2-μm fractions showed a broad, single endotherm at 562°C, with a 12.6% weight loss due to dehydroxylation, and a sharp exotherm at 998°C due to the recrystallization reaction. An endothermic peak appeared at 679°C, and grew larger with increasing particle

Dickite

Figure 3b shows an XRD pattern of a random mount dickite sample. The d-values and relative intensities agree well with the data for dickite reported by Bailey (1963). The cell parameters, calculated by least-squares

Table 3. Chemical analyses of mica.

|	1	2	3
SiO_2	48.25	47.14	47.65
Al_2O_3	33.91	37.09	37.03
TiO_2	0.22	0.34	0.10
Fe_2O_3	1.09	0.49	0.01
MgO	0.32	0.83	0.04
CaO	0.01	0.57	—
Na_2O	0.06	0.35	0.76
K_2O	9.04	7.10	9.02
H_2O (+)	6.28	5.18	4.97
H_2O (−)	1.41	0.99	0.73
Total (%)	100.59	100.09	100.33

(1) Specimen from Makurazaki, Kagoshima Prefecture, Japan. (2) $2M_2$ mica from Akita Prefecture, Japan (Shimoda, 1970). Total includes 0.01% P_2O_5. (3) $2M_1$ mica from Yoji Pass, Gunma Prefecture, Japan (Sudo, 1978). Total includes 0.02% P_2O_5.

size (Figure 5). Hill (1955) has reported the development of a 14 Å-phase dickite on dehydroxylation. Brindley and Wan (1978) found that structurally well-ordered dickites give maximum development of a 14 Å phase on heating, but that less well-ordered dickites show little or no development of this phase. The 14 Å phase appeared for our dickite sample at 550°C, and remained up to 800°C.

The dickite particles exhibit a euhedral rhombic-shaped habit. Hexagonal-shaped particles were rarely observed (Figure 4b).

$2M_2$ mica

An XRD pattern of the $2M_2$ mica is shown in Figure 3c. The pattern clearly indicates that the specimen is the $2M_2$ polytype. The XRD pattern of the oriented material shows basal reflections at 10.2, 5.02, 3.34, 2.57, and 2.01 Å, in the air-dried state under 50% relative humidity (RH). These peaks shifted slightly to 10.0, 5.05, 3.35, 2.50, and 2.01 Å after ethylene glycol solvation, and to 10.0, 5.00, 3.33, 2.50, and 1.99 Å after heating at 500°C for 1 hr. This behavior implies that the specimen contains a small amount of expandable layers. The d(060) value is 1.497 Å, indicating a dioctahedral structure. The chemical analyses of the specimen and other related materials are given in Table 3. The structural formula is:

$$(K_{0.77}Na_{0.01})(Al_{1.91}Fe^{3+}_{0.05}Mg_{0.03}Ti_{0.01})-$$
$$(Si_{3.23}Al_{0.77})O_{10}(OH)_2.$$
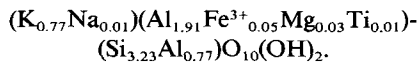
The negative layer charge of the material is $-0.78/O_{10}(OH)_2$ and originates from substitution of Al^{3+} for Si^{4+} in the tetrahedral sheet. The value is slightly smaller than the theoretical value for muscovite and agrees with that for clay micas of hydrothermal origin (Higashi, 1980). The DTA and TGA curves show a very small endotherm at 60°C due to the loss of adsorbed water, and/or interlayer water from small amounts of expandable layers. A large endotherm at 605°C is due
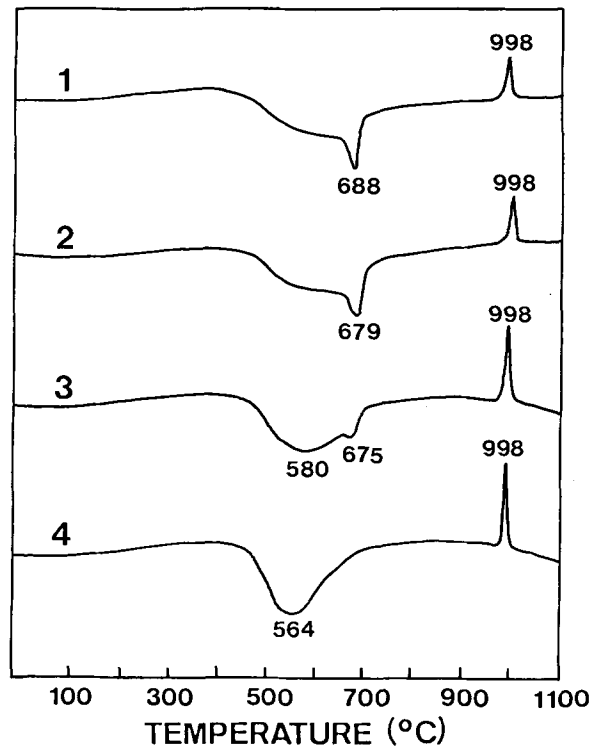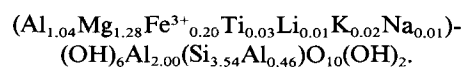

Figure 5. Differential thermal analysis curves for various dickite samples. (1) 50–20 μm, (2) 20–5 μm, (3) 5–2 μm, (4) <2 μm.

to the dehydroxylation of structural OH. The IR spectrum has an OH-absorption band at 3640 cm^{-1}, with a broad shoulder at 3658 cm^{-1}. The material has a euhedral, lath-shaped habit (Figure 4c).

Sudoite

Figure 4d shows an XRD pattern of a random mount sudoite sample. The pattern demonstrates that the specimen is the IIb polytype. The d-values for the basal reflections did not change with ethylene glycol solvation, but shifted slightly to smaller values after heating at 700°C for 1 hr. The d(060) value is 1.508 Å, indicating a dioctahedral structure. The cell parameters calculated by least-squares refinement are: $a_0 = 5.223(2)$, $b_0 = 9.047(3)$, $c_0 = 14.314(8)$ Å, and $\beta = 97.07(5)°$. The chemical composition is given in Table 4, together with those of other related materials from the Kamikita mine (Hayashi and Oinuma, 1964) and the Itaya Roseki deposit (Shirozu, 1978). The specimen from Makurazaki is chemically similar to the material from the Kamikita mine, which belongs to Kuroko deposit (Hayashi and Oinuma, 1964). A structural formula calculated by assuming that the octahedral sheet in the 2:1 layer is occupied by Al is:
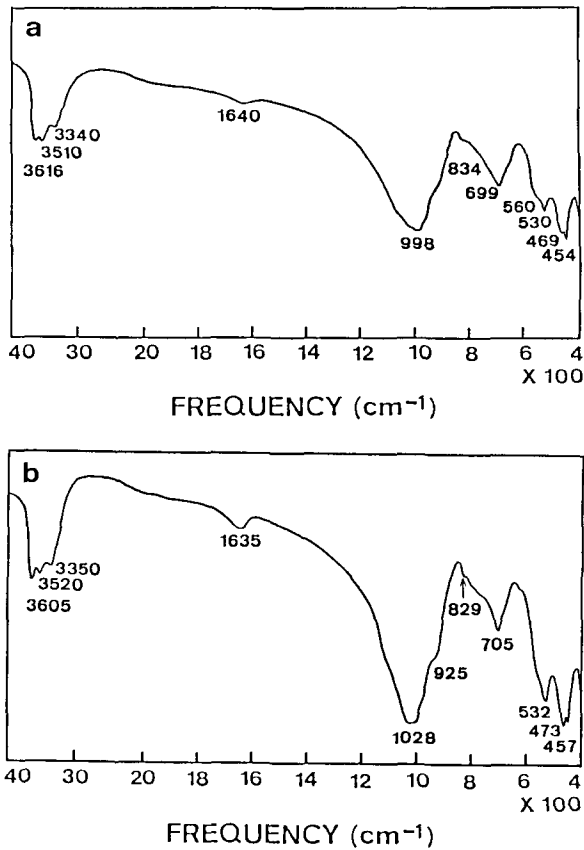
$$(Al_{1.04}Mg_{1.28}Fe^{3+}_{0.20}Ti_{0.03}Li_{0.01}K_{0.02}Na_{0.01})-$$
$$(OH)_6Al_{2.00}(Si_{3.54}Al_{0.46})O_{10}(OH)_2.$$

Figure 6.   Infrared absorption spectra for (a) sudoite and (b) tosudite.

Table 4.   Chemical analyses of Al-chlorite.

	1	2	3
SiO_2	39.25	35.63	43.43
Al_2O_3	32.94	34.87	39.21
TiO_2	0.48	—	—
Fe_2O_3	2.98	5.01	0.17
FeO		0.43	
MnO	—	0.05	—
MgO	9.49	8.63	0.13
CaO	0.01	1.13	0.47
Na_2O	0.08	0.24	1.41
K_2O	0.17	0.46	0.49
Li_2O	0.02	—	1.43
H_2O (+)	6.28	12.24	11.59
H_2O (−)	1.41	1.91	1.47
Total (%)	100.03	100.60	99.91

(1) Specimen from Makurazaki, Kagoshima Prefecture, Japan. (2) Sudoite from Kamikita mine (Kuroko deposit), Aomori Prefecture, Japan (Hayashi and Oinuma, 1964). (3) Donbasite from Itaya (Roseki deposit), Okayama Prefecture, Japan (Shirozu, 1978). Total includes 0.11% P_2O_5.

The DTA and TGA curves show a large endothermic peak at 586°C and a small, broad peak at 785°C, accompanying the 10 and 1% weight losses, respectively. The IR spectrum shows three absorption bands at 3616, 3510, and 3340 cm^{-1} (Figure 6a). These bands are believed to be characteristic absorptions for OH in dioctahedral chlorite (Oinuma and Hayashi, 1966; Hayashi and Oinuma, 1967). Shirozu and Higashi (1976) suggested that the three bands may be caused by differences in the OH–O distances due to corrugation of the basal oxygen surface. According to Shirozu and Ishida (1982), the band at 699 cm^{-1} is due to an interlayer O-OH vibration, as it disappeared after heating at 600°C for 1 hr. The band at 550 cm^{-1} is due to the Si–O–Al^{VI} vibration (Stubičan and Roy, 1961a, 1961b). These absorptions are quite similar to those of sudoite from the Kamikita mine (Hayashi and Oinuma, 1964, 1965). The material is composed of euhedral platelets with irregular outlines (not shown).
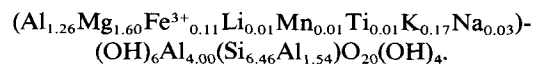
Tosudite

Figure 7 shows the XRD patterns of an oriented tosudite sample, before and after ethylene glycol solvation of 50% RH. The untreated material shows the
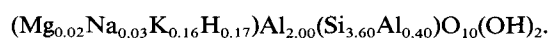
(001) reflection at 30.2 Å, and a regular series of higher order. The average basal spacing, calculated from the 12 basal reflections, and excluding the first-order peak, is 29.77 Å. The average basal spacing expanded to 31.37 Å after the solvation. The d(060) value is 1.506 Å. A chemical analysis of the specimen is given in Table 5, together with relevant data taken from previous studies. The chemical composition is closer to that of a tosudite from the Kuroko deposit (Kitakami mine; Sudo and Kodama, 1957) than from the Roseki deposit (Tooho mine; Nishiyama *et al.*, 1975). Although the material is composed of Al-rich chlorite and dioctahedral smectite layers, the detailed cation distributions between both octahedral sheets of the chlorite layers are uncertain. The structural formula was calculated by assuming that the octahedral sheet in the 2:1 layer is occupied by Al. The formula is:

$$(Al_{1.26}Mg_{1.60}Fe^{3+}_{0.11}Li_{0.01}Mn_{0.01}Ti_{0.01}K_{0.17}Na_{0.03})-$$
$$(OH)_6Al_{4.00}(Si_{6.46}Al_{1.54})O_{20}(OH)_4.$$

The exchangeable cations extracted with a 0.1 N $SrCl_2$ solution are 0.79% K_2O, 0.08% Na_2O, and 0.05% MgO. The CEC value is 40.8 meq/100 g. The structural formulae of component layers were calculated by assuming that the CEC originates from the negative charge of the expandable layer and the hydrogen ion compensates for the deficiency of the positive charge of the exchangeable cations. The structural formula for the chlorite layer is:

$$(Al_{1.26}Mg_{1.58}Fe^{3+}_{0.11}Li_{0.01}Mn_{0.01}Ti_{0.01}K_{0.01})-$$
$$(OH)_6Al_{2.00}(Si_{2.86}Al_{1.14})O_{10}(OH)_2,$$
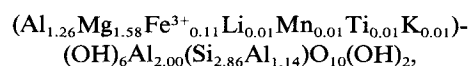
and that for the expandable layer is:

$$(Mg_{0.02}Na_{0.03}K_{0.16}H_{0.17})Al_{2.00}(Si_{3.60}Al_{0.40})O_{10}(OH)_2.$$

The relatively large amounts of Mg and very small

Table 5. Chemical analyses of tosudite.

	1	2	3
SiO_2	39.41	39.94	41.60
Al_2O_3	35.24	33.17	36.40
TiO_2	0.04	0.74	—
Fe_2O_3	0.89	1.34	1.82
FeO	—	0.18	—
MnO	0.04	—	—
MgO	6.54	6.44	0.29
CaO	0.01	1.30	0.38
Na_2O	0.09	0.52	0.14
K_2O	0.83	0.24	0.38
Li_2O	0.01	—	1.04
H_2O (+)	12.49	11.64	11.12
H_2O (−)	4.81	4.39	6.87
Total (%)	100.40	99.98	100.04

(1) Specimen from Makurazaki, Kagoshima Prefecture, Japan. (2) Tosudite from Kitakami mine (Kuroko deposit), Aomori Prefecture, Japan (Sudo and Kodama, 1957). Total inclues 0.08% P_2O_5 and 0.69% S. (3) Tosudite from Tooho mine (Roseki deposit), Aichi Prefecture, Japan (Nishiyama et al., 1975).

Figure 7. X-ray powder diffraction patterns of oriented tosudite (a) before and, (b) after ethylene glycol solvation.
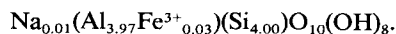
amounts of Li suggest that the chlorite layer belongs to sudoite rather than donbasite or cookeite. The structural formula of the expandable layer is compatible with a beidellite with a negative charge of −0.40/$O_{10}(OH)_2$.

In DTA and TGA, the mineral has a double endothermic peak at 70 and 128°C, accompanied by a 7.5% weight loss, which is attributed to the dehydration of the expandable layers. A large endothermic peak at 572°C is due to the dehydroxylation reaction. The DTA and TGA curves resemble those of the sudoite mentioned above, except for the endotherm due to the dehydration of interlayer water. Figure 6b shows the IR spectrum of the tosudite sample. The three OH-vibration bands at 3605, 3520, and 3350 cm^{-1} are clearly observed. Subhedral, irregular-shaped particles similar to those of the sudoite are seen in the electron microscope.

MINERALOGY OF CLAYS IN THE L-TYPE ALTERATION AUREOLE

Kaolinite

Figure 8a shows an XRD pattern of a random mount kaolinite sample. The Hinckley index is 0.76, indicating a poorly ordered structure. The structural formula, calculated from the chemical analysis (Table 6), is:

$$Na_{0.01}(Al_{3.97}Fe^{3+}{}_{0.03})(Si_{4.00})O_{10}(OH)_8.$$

The DTA and TGA curves exhibit a dehydroxylation endotherm at 544°C accompanying a 13.8% weight loss. An exotherm at 992°C is due to the recrystallization reaction. The IR spectrum shows three OH-vibration bands at 3700, 3656, and 3625 cm^{-1}. The intensities of the absorptions at 3700 (A_{outer}) and 3625
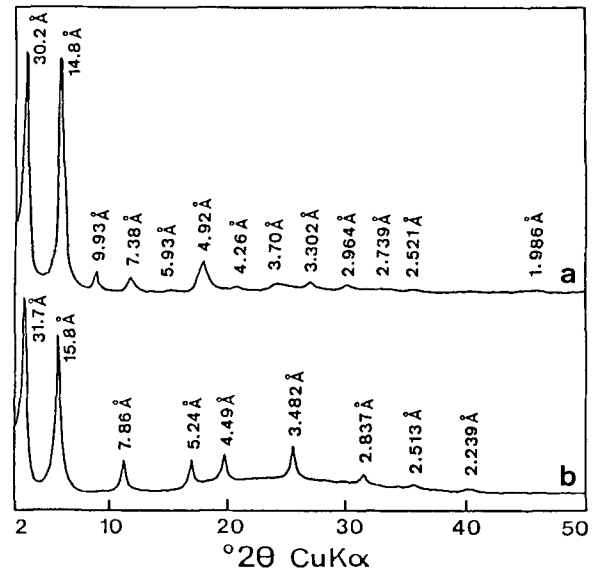
cm^{-1} (A_{inner}) are: $A_{outer} > A_{inner}$; quite different from the dickite described above.

Rectorite

XRD patterns of the rectorite before and after ethylene glycol solvation at 50% RH are given in Figures 8 (b, c). The average basal spacings, calculated from all basal reflections, excluding the first order, are 25.47 Å for the natural state, and 26.79 Å after solvation. The d(060) value is 1.496 Å, indicating a dioctahedral structure. According to the diagram of Tomita et al. (1989), the interstratification can be expressed by Reichweite g = 1 and the ratios of component layers are 55 and 45% for mica and smectite layers, respectively. The chemical composition of the rectorite is

Table 6. Chemical analyses of kaolinite.

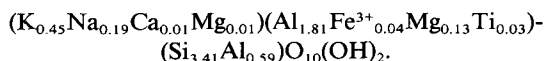|	1	2	3
SiO_2	46.22	43.58	45.2
Al_2O_3	38.95	38.82	39.2
TiO_2	0.04	0.49	1.21
Fe_2O_3	0.37	0.43	0.17
MgO	0.02	0.43	0.08
CaO	0.00	0.25	0.06
Na_2O	0.03	0.29	0.03
K_2O	0.04	0.26	0.02
H_2O (+)	14.10	14.34	13.3
H_2O (−)	0.02	0.98	
Total (%)	99.79	99.87	99.27

(1) Specimen from Makurazaki, Kagoshima Prefecture, Japan. (2) Kaolinite from Niida, Akita Prefecture, Japan (Kimbara and Nagata, 1974). (3) Kaolinite from Washington County, Georgia (Jepson and Rowse, 1975). Contains 1–2% anatase.

Table 7. Chemical analyses of rectorite.

	1	2	3
SiO_2	48.33	46.46	52.62
Al_2O_3	28.69	29.75	29.08
TiO_2	0.61	0.67	0.12
Fe_2O_3	0.75	1.65	0.19
FeO	—	—	0.52
MnO	—	—	0.06
MgO	1.30	0.58	0.77
CaO	0.14	0.34	0.51
Na_2O	1.41	2.92	0.10
K_2O	4.94	2.17	4.44
H_2O (+)	6.22	6.01	5.52
H_2O (−)	7.47	8.96	6.25
Total (%)	99.92	99.51	100.08

(1) Specimen from Makurazaki, Kagoshima Prefecture, Japan. (2) Na-rectorite from Makurazaki, Kagoshima Prefecture, Japan (Kawano and Tomita, 1989). (3) K-rectorite from Tulameen coalfield, British Colombia (Pevear *et al.*, 1980).

Table 8. Chemical analyses of smectite.

	1	2	3
SiO_2	48.77	48.24	59.30
Al_2O_3	20.02	17.01	36.11
TiO_2	0.82	0.02	—
Fe_2O_3	1.89	0.81	0.50
FeO	—	0.15	—
MgO	1.95	4.05	0.10
CaO	0.88	3.03	0.02
Na_2O	1.02	0.34	3.98
K_2O	0.96	0.16	0.11
H_2O (+)	9.33	8.59	
H_2O (−)	13.72	17.21	
Total (%)	99.54	99.30	100.12

(1) Specimen from Makurazaki, Kagoshima Prefecture, Japan. (2) Montmorillonite from Cheto, Arizona (Takeshi and Uno, 1979). (3) Beidellite from Black Jack mine, Owyhee County, Idaho (Weir, 1956).

characterized by a large K_2O content (Table 7). The structural formula calculated from the chemical analysis is:

$$(K_{0.45}Na_{0.19}Ca_{0.01}Mg_{0.01})(Al_{1.81}Fe^{3+}_{0.04}Mg_{0.13}Ti_{0.03})-$$
$$(Si_{3.41}Al_{0.59})O_{10}(OH)_2.$$

The formula reveals that the sample is rich in K and Al, and is relatively poor in Na and Mg. This implies that the material is composed of a regular interstratification of K-mica-like and beidellite-like layers.

The DTA curve exhibits endothermic peaks at 81 and 184°C due to the removal of interlayer water and dehydroxylation at 568°C. The Na-rectorite studied by Kawano and Tomita (1989) was also collected from the rectorite zone of the L-type hydrothermal alteration aureole in the Makurazaki area. The Na-rectorite has greater regularity of interstratification and a higher Na content than does the present material. The K-rectorite sample also rehydrated easily on water saturation after heating at 800°C for 1 hr, and showed similar rehydration behavior to the Na-rectorite. The strong rehydration properties support the idea that the expandable layer of the K-rectorite has a beidellite-like composition (Kawano and Tomita, 1991). The morphology of the material is irregular in habit.
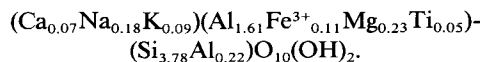
Smectite

XRD patterns of the smectite before and after ethylene glycol solvation at 50% RH are shown in Figures 8 d, e. The average basal spacings are 15.08 Å for the natural state, and 16.88 Å after the solvation. The d(060) spacing is 1.494 Å, confirming that the material is dioctahedral. The chemical analysis of the smectite is given in Table 8, together with those of Cheto montmorillonite (Takeshi and Uno, 1979) and the beidellite from the Black Jack mine (Weir, 1965). The structural

formula calculated from the chemical analysis is:

$$(Ca_{0.07}Na_{0.18}K_{0.09})(Al_{1.61}Fe^{3+}_{0.11}Mg_{0.23}Ti_{0.05})-$$
$$(Si_{3.78}Al_{0.22})O_{10}(OH)_2.$$

The formula indicates that the specimen has a composition intermediate between montmorillonite and beidellite. The DTA curve shows endotherms at 98 and 172°C, which are attributed to the loss of interlayer water, and a single endotherm at 667°C due to the loss of structural OH. Thin particles with irregular outlines are seen in the electron microscope.

DISCUSSION

Two distinct zonal sequences of clay minerals (H- and L-type) can be observed around the silicified rocks in the Makurazaki volcanic area. According to Fujii and Inoue (1971), the pyrophyllite deposit can be divided into two type based on elements concentrated at the center of the alteration aureole. One is Al-concentrated, the other is Si-concentrated. A solubility diagram for the Al_2O_3-SiO_2-H_2O system (Tsuzuki, 1976) shows that these differences at the center of the alteration aureole are affected by the acidity of the fluids. Based on this result, both H- and L-type alteration aureoles in the Makurazaki area also appear to have been formed by reaction with strongly acidic fluids.

The fluids dissolving the elements of the wall rocks (other than Si) moved toward the margins, and pH values probably increased. The solubility of Al decreased with decreasing acidity of the fluids, and precipitation of Al occurred as pyrophyllite, dickite, or kaolinite as the temperature of the fluid decreased. Eberl and Hower (1975) proposed two conversion reactions from kaolinite to pyrophyllite: 1. kaolinite + 2(quartz) → pyrophyllite + H_2O; and 2. 2(kaolinite) → pyrophyllite + 2(boehmite) + $2H_2O$. They reported equilibrium temperatures of 345°C for the first reaction and 405°C for the second, under 2 kbar water pressure.
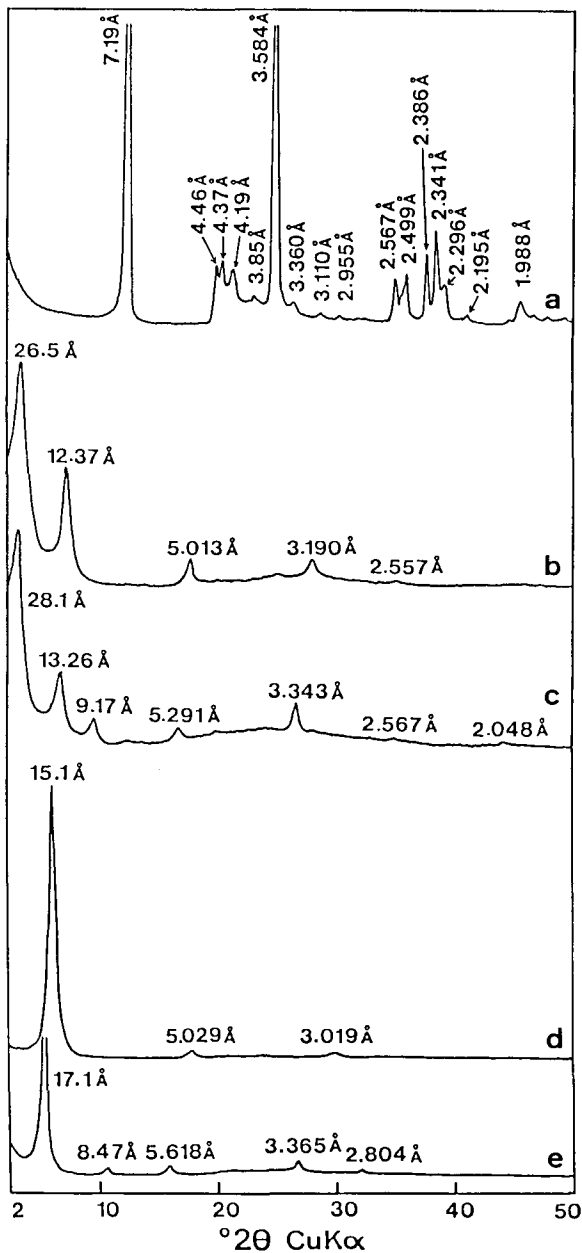
Figure 8.   X-ray powder diffraction patterns of (a) randomly-oriented kaolinite, oriented rectorite (b) before and, (c) after ethylene glycol solvation, and oriented smectite (d) before and, (e) after solvation.
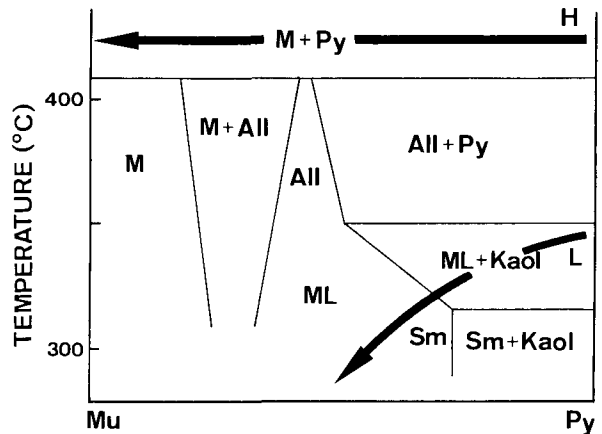

Figure 9.   Hydrothermal reaction series of H- and L-type alteration aureoles represented on the stability diagram of Velde (1969). Py = pyrophyllite, Mu = muscovite, All = allevardite, M = mica, ML = randomly interstratified phase, Sm = smectite, Kaol = kaolinite.

Henmi and Matsuda (1975) reported that the boundary temperatures are 263°C, 1 kbar and 270°C, 2 kbar for the first reaction, and 333°C, 1 kbar and 340°C, 2 kbar for the second reaction. The boundary temperatures determined by these authors are significantly different. However, both reactions indicated that the stable temperature of pyrophyllite is apparently higher than that of kaolinite. Accurate equilibrium conditions between dickite and pyrophyllite and between dickite and kaolinite remain uncertain. However, many reports of natural occurrences of these minerals indicate stable temperatures for dickite slightly higher than those for kaolinite (Tokunaga, 1954, 1955, 1957), and apparently lower than those for pyrophyllite (Schroeder and Hays, 1967; Uno and Takeshi, 1982; Inoue and Utada, 1989). This suggests that the H-type alteration aureole formed under higher temperatures than the L-type aureole.

Velde (1969) constructed a muscovite-pyrophyllite phase diagram for various P-T and K-activity conditions. The two types of hydrothermal alteration in the Makurazaki area can be represented as arrows on Velde's diagram, as shown in Figure 9. The H-type reaction is characterized by the formation of mica from pyrophyllite, without allevardite or interstratified phases. It can be categorized as a high-temperature reaction. The L-type reaction is characterized by the formation of fully-expandable phases (smectite) from kaolinite through an interstratified phase (rectorite). This type can be categorized as a low-temperature reaction. Eberl (1978a, 1978b) reported that K-smectite changes to mica through K-rectorite with increasing temperature, and that the small hydration energy of K plays an important role in the formation of collapsed layers. These results suggest that the mica in the H-type alteration zone, and the rectorite and smectite in the L-type alteration zone were formed in order of temperature and K-activity conditions: mica > rectorite > smectite for temperature; mica > rectorite > smectite for K-activity.

Shimoda et al. (1977) summarized the relationship between mode of occurrence and mineralogical properties of sudoite and tosudite. They indicated that the
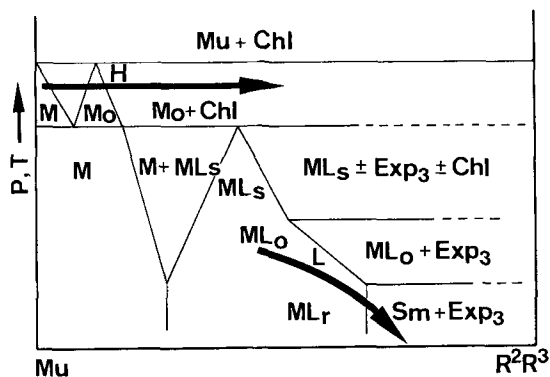
Figure 10. Hydrothermal reaction series of H- and L-type alteration aureoles represented on the stability diagram of Velde (1985). Mu = muscovite, Chl = chlorite, M = mica, Mo = IMII phase, ML_s = allevardite, ML_o = ordered mixed-layer phase, ML_r = random mixed-layer phase, Sm = smectite, Exp_3 = trioctahedral expanding phase.

minerals occurring in the Toseki and Roseki deposits can be characterized by very small amounts of Mg and relatively large amounts of Li ($LiO_2 = 1.16$–0.60 wt. %), whereas those in the Kuroko ore deposits contain relatively large amounts of Mg and very small amounts of Li. The materials collected from Makurazaki contain large amounts of Mg and small amounts of Li, suggesting a similar chemical composition to those from the Kuroko deposits (Sudo and Kodama, 1957; Shirozu, 1978). Sudoite and tosudite often occur together with kaolinite (Brown et al., 1974; Kanaoka, 1975; Ichikawa and Shimoda, 1976; Merceron et al., 1988) and mica or interstratified mica/smectite (Tsukahara, 1964; Nishiyama et al., 1975; Higashi, 1990). The formation conditions of the minerals are poorly understood. In Makurazaki, sudoite and tosudite occurred at the periphery of the mica zone in the H-type alteration aureole. The formation of sudoite as plotted on the Velde diagram is shown in Figure 10. The H-type alteration on the diagram shows that sudoite was formed with decreasing K-activity due to the crystallization of mica, and increasing Mg-activity under high temperature conditions. Smectite in the L-type alteration was formed with decreasing K-activity and increasing Mg-activity under low-temperature conditions. Kramm (1980) noted that the sudoite associated with quartz veins in the Harz was formed about 360°C at 1–2 kbar. Fransolet and Schreyer (1984), on the other hand, pointed out that a stability field of sudoite ranges from about 150° to 350°C at 1 kbar. Matsuda and Henmi (1973) reported that mica/smectite interstratified minerals transformed into tosudite in pure water at about 360°C at 1 kbar. Matsuda and Henmi (1974), however, synthesized tosudite (they used the term "30 Å-interstratified mineral") from kaolin in the presence of various cations. They pointed out that tosudite was formed in the fluids containing Mg or Li ions between 420°

and 520°C at 1 kbar. Furthermore, Matsuda et al. (1990) reported that tosudite was synthesized from Mg-, Li-, Ni-, and Co-saturated dioctahedral smectites at 400–500°C. These results all suggest that sudoite and tosudite should be formed under relatively high temperatures and high Mg- or Li-activities.

ACKNOWLEDGMENTS

REFERENCES

Bailey, S. W. (1963) Polymorphism of the kaolin minerals: *Amer. Mineral.* **48**, 1196–1209.

Brindley, G. W. and Wan, Hsien-Ming (1978) The 14 Å phase developed in heated dickites: *Clay Miner.* **13**, 17–23.

Brindley, G. W. and Wardle, R. (1970) Monoclinic and triclinic forms of pyrophyllite and pyrophyllite anhydride: *Amer. Mineral.* **55**, 1259–1272.

Brown, G., Bourguignon, P., and Thorez, J. (1974) A lithium-bearing aluminian regular mixed layer montmorillonite-chlorite from Huy, Belgium: *Clay Miner.* **10**, 135–144.

Deer, W., Howie, R. A., and Zussman, J. (1962) *Rock Forming Minerals, Vol. 3, Sheet Silicates:* Longmans, London, 270 pp.

Eberl, D. and Hower, J. (1975) Kaolinite synthesis: The role of the Si/Al and (alkali)/(H$^+$) ratio in hydrothermal systems: *Clays & Clay Minerals* **23**, 301–309.

Eberl, D. (1978a) Reaction series for dioctahedral smectite: *Clays & Clay Minerals* **26**, 327–340.

Eberl, D. (1978b) The reaction of montmorillonite to mixed-layer clay: The effect of interlayer alkaline earth cations: *Geochim. Cosmochim. Acta* **42**, 1–7.

Farmer, V. C. and Russell, J. D. (1964) The infrared spectra of layer silicates: *Spectrochim. Acta* **20**, 1149–117.

Fransolet, A. M. and Schreyer, W. (1984) Sudoite, di/trioctahedral chlorite: A stable low-temperature phase in the system MgO-Al$_2$O$_3$-H$_2$O: *Contrib. Mineral. Petrol.* **86**, 409–417.

Fujii, N. and Inoue, I. (1971) Geologic features and classification of the pyrophyllite deposits in the Hokushin district, Central Japan: *Mining Geol.* **21**, 407–417 (in Japanese).

Hayashi, H. and Oinuma, K. (1964) Aluminian chlorite from Kamikita mine, Japan: *Clay Sci.* **2**, 22–30.

Hayashi, H. and Oinuma, K. (1965) Relationship between infrared absorption spectra in the region of 450–900 cm⁻¹ and chemical composition of chlorite: *Amer. Mineral.* **50**, 476–483.

Hayashi, H. and Oinuma, K. (1967) Si-O absorption bands near 1000 cm⁻¹ and OH absorption bands of chlorites: *Amer. Mineral.* **52**, 1206–1210.

Henmi, K. and Matsuda, T. (1975) The equilibrium boundaries between kaolinite and pyrophyllite: in *Contributions to Clay Mineralogy, Dedicated to Prof. Toshio Sudo on the Occasion of his Retirement,* K. Henmi, ed., Prof. Sudo Retirement Ceremony Organization, Tokyo, 151–156.

Higashi, S. (1980) Mineralogical studies of hydrothermal dioctahedral mica minerals: *Memo. Fac. Sci. Kochi Univ.* **1**, 1–39.

Higashi, S. (1990) Li-tosudite in Tobe pottery stone: *J. Mineral. Soc. Japan. Spec. Issue* **19**, 3–9 (in Japanese).

Hill, R. D. (1955) 14 Å spacings in kaolin minerals: *Acta Crystallogr.* **8**, 120.

Ichikawa, A. and Shimoda, S. (1976) Tosudite from the Hokuno mine, Hokuno, Gifu Prefecture, Japan: *Clays & Clay Minerals* **24**, 142–148.

Inoue, A. and Utada, M. (1989) Mineralogy and genesis of hydrothermal aluminous clays containing sudoite, tosudite, and rectorite in a drillhole near the Kamikita Kuroko ore deposit, northern Honshu, Japan: *Clay Sci.* **7**, 193–217.

Izawa, E., Urashima, Y., and Okubo, Y. (1984) Age of mineralization of the Nansatsu type gold deposits, Kagoshima, Japan—K-Ar dating of alunite from Kasuga, Iwato and Akeshi: *Mining Geol.* **34**, 343–351 (in Japanese).

Jepson, W. B. and Rowse, J. B. (1975) The composition of kaolinite—An electron microscope microprobe study: *Clays & Clay Minerals* **23**, 310–317.

Kanaoka, S. (1975) Tosudite-like clay minerals in pottery stone: in *Contributions to Clay Mineralogy, Dedicated to Prof. Toshio Sudo on the Occasion of his Retirement*, K. Henmi, ed., Prof. Sudo Retirement Ceremony Organization, Tokyo, 34–41 (in Japanese).

Kawano, M., Tomita, K., Yamamoto, M., and Oba, N. (1986) Clay minerals, especially on interstratified minerals, in and around Makurazaki area, Kagoshima Prefecture, Japan: *Rept. Fac. Sci. Kagoshima Univ.* **19**, 45–66 (in Japanese).

Kawano, M. and Tomita, K. (1989) Rehydration properties of Na-rectorite from Makurazaki, Kagoshima Prefecture, Japan: *Miner. J. (Tokyo)* **14**, 351–372.

Kawano, M. and Tomita, K. (1991) X-ray powder diffraction studies on the rehydration properties of beidellite: *Clays & Clay Minerals* **39**, 77–83.

Kimbara, K. and Nagata, H. (1974) Clay minerals in the core samples of the mineralized zone at Niida, southern part of Odate, Akita Prefecture, Japan, with special reference of the mineralogical properties of sudoite and tosudite: *J. Japan Assoc. Min. Petr. Econ. Geol.,* **69**, 239–254.

Kodama, H. (1958) Mineralogical study on some pyrophyllite in Japan: *Miner. J. (Tokyo)* **2**, 236–244.

Kramm, U. (1980) Sudoite in low-grade metamorphic manganese rich assemblages: *N. Jahrb. Mineral. Abh.* **138**, 1–13.

Ledoux, R. L. and White, J. L. (1964a) Infrared study of the OH groups in expanded kaolinite: *Science* **143**, 244–246.

Ledoux, R. L. and White, J. L. (1964b) Infrared study of selective deuteration of kaolinite and halloysite at room temperature: *Science* **145**, 47–49.

Matsuda, T. and Henmi, K. (1973) Hydrothermal behavior of an interstratified mineral from the Mine of Ebara, Hyogo Prefecture, Japan. (An example of change from randomly interstratified clay mineral to regular one): *Nendo Kagaku (J. Clay Sci. Soc. Japan)* **13**, 87–94 (in Japanese).

Matsuda, T. and Henmi, K. (1974) Syntheses of interstratified minerals from kaolin with addition of various cations: *J. Mineral. Soc. Japan Spec. Issue* **11**, 152–161 (in Japanese).

Matsuda, T., Yoshida, M., Hamada, Y., and Ossaka, J. (1990) Hydrothermal behaviors of dioctahedral smectites: *J. Mineral. Soc. Japan Spec. Issue* **19**, 107–111 (in Japanese).

Merceron, T., Inoue, A., Bouchet, A., and Meunier, A. (1988) Lithium-bearing donbasite and tosudite from Echassieres, Massif Central, France: *Clays & Clay Minerals* **36**, 39–46.

Nishiyama, T., Shimoda, S., Shimosaka, K., and Kanaoka, S. (1975) Lithium-bearing tosudite: *Clays & Clay Minerals* **23**, 337–342.

Oinuma, K. and Hayashi, H. (1966) Infrared study of clay minerals from Japan: *J. Tokyo Univ., Gen. Education (Nat. Sci.)* **6**, 1–15.

Pevear, D. R., Williams, V. E., and Mustoe, G. E. (1980) Kaolinite, smectite and K-rectorite in bentonites: Relation to coal rank at Tulameen, British Columbia: *Clays & Clay Minerals* **28**, 241–254.

Schmidt, E. R. and Heckroodt, R. O. (1959) A dickite with an elongated crystal habit and its dehydroxylation: *Mineral. Mag.* **32**, 314–323.

Schroeder, R. and Hayes, J. B. (1967) Dickite and kaolinite in Pennsylvania limestones of southeastern Kansas: *Clays & Clay Minerals* **16**, 41–49.

Shimoda, S. (1970) A hydromuscovite from the Shakanai mine, Akita Prefecture, Japan: *Clays & Clay Minerals* **18**, 269–274.

Shimoda, S., Nishiyama, T., Kitani, S., and Ichikawa, A. (1977) Mode of occurrence and mineralogical properties of tosudite: *J. Mineral. Soc. Japan Spec. Issue* **13**, 103–110 (in Japanese).

Shirozu, H. and Higashi, S. (1976) Structural investigations of sudoite and regularly interstratified sericite/sudoite: *Miner. J. (Tokyo)*, **8**, 158–170.

Shirozu, H. (1978) Chlorite minerals: in *Clays and Clay Minerals of Japan*, T. Sudo and S. Shimoda, eds., Elsevier, Amsterdam, 243–264.

Shirozu, H. and Ishida, K. (1982) Infrared study of some 7 Å and 14 Å layer silicates by deuteration: *Miner. J. (Tokyo)* **11**, 161–171.

Smithson, F. and Brown, G. (1957) Dickite from sandstones in northern England and North Wales: *Mineral. Mag.* **31**, 381–389.

Stubičan, V. and Roy, R. (1961a) A new approach to the assignment of infrared absorption bands in layer silicates: *Z. Kristallogr.* **115**, 200–214.

Stubičan, V. and Roy, R. (1961b) Isomorphous substitution and infrared spectra of the layer lattice silicates: *Amer. Mineral.* **46**, 32–51.

Sudo, T. and Kodama, H. (1957) An aluminian mixed-layer mineral of montmorillonite-chlorite: *Z. Kristallogr.* **190**, 379–387.

Sudo, T. (1978) An outline of clays and clay minerals in Japan: in *Clays and Clay Minerals of Japan*, T. Sudo and S. Shimoda, eds., Elsevier, Amsterdam, 1–103.

Takeshi, H. and Uno, Y. (1979) Notes on the formation and transformation of montmorillonites in Japan: *J. Miner. Soc. Japan Spec. Issue* **14**, 70–77 (in Japanese).

Tokunaga, M. (1954) Geology and ore deposits of the Kasuga mine and Akeshi mine, in the Makurazaki district, Kagoshima Prefecture: *Mining Geol.* **4**, 205–212 (in Japanese).

Tokunaga, M. (1955) Fundamental studies of the hydrothermal alteration at the Kasuga mine, Kagoshima Prefecture, Japan: *Mining Geol.* **5**, 1–8 (in Japanese).

Tokunaga, M. (1957) Nacrite-bearing kaolin clay from the Kasuga mine, Kagoshima Prefecture, Japan: *Miner. J. (Tokyo)* **2**, 103–113.

Tomita, K. and Dozono, M. (1973) An expansible mineral having high rehydration ability: *Clays & Clay Minerals* **21**, 185–190.

Tomita, K., Takahashi, H., and Watanabe, T. (1989) Quantification curves for mica/smectite interstratifications by X-ray powder diffraction: *Clays & Clay Minerals* **36**, 258–262.

Tsukahara, N. (1964) Dioctahedral chlorite from the Furutobe mine, Akita Prefecture, Japan: *Clay Sci.* **2**, 56–75.

Tsuzuki, Y. (1976) Solubility diagrams for explaining zone sequences in bauxite, kaolin and pyrophyllite-diaspore deposits: *Clays & Clay Minerals* **24**, 297–302.

Ueno, M. (1964) On some kaolin-roseki deposits in northern part of Hyogo Prefecture: *Bull. Geol. Surv. Japan* **15**, 235–250 (in Japanese).

Uno, Y. and Takeshi, H. (1982) Rock alteration and formation of clay minerals in the Ugusu silica deposit, Izu Peninsula, Japan: *Clay Sci.* **6**, 9–42.

Urashima, Y., Saito, M., and Sato, E. (1981) The Iwato gold

ore deposits, Kagoshima Prefecture, Japan. *Mining Geol., Spec. Issue* **10**, 1–14.

Urashima, Y., Izawa, E., and Hedenquist, J. W. (1987) Nansatsu-type gold deposits in the Makurazaki district: in *Gold Deposits and Geothermal Fields in Kyushu,* Y. Urashima, ed., The Society of Mining Geologists of Japan, Tokyo, 13–22.

Velde, B. (1969) The compositional join muscovite-pyrophyllite at moderate temperatures and pressures: *Bull. Soc. Franc. Miner. Crystallogr.* **92**, 360–368.

Velde, B. (1985) General phase diagram for some clay mineral assemblages: in *Clay Minerals, A Physico-Chemical Explanation of their Occurrence,* B. Velde, ed., Elsevier, Amsterdam, 257–359.

Wada, K. (1967) A study of hydroxyl groups in kaolin minerals utilizing selective deuteration and infrared spectroscopy: *Clay Miner.* **7**, 51–61.

Weir, A. H. (1965) Potassium retention in montmorillonite: *Clay Miner.* **6**, 17–22.